ECOLOGICAL ENGINEERING & ENVIRONMENTAL TECHNOLOGY

Ecological Engineering & Environmental Technology, 2026, 27(10), 401–414
https://doi.org/10.12912/27197050/235784
ISSN 2719–7050, License CC-BY 4.0

Received: 2026.08.01
Accepted: 2026.09.03
Published: 2026.09.10

Assessment of the influence of meteorological and vehicular factors on the deposition of atmospheric sedimentable dust in Huánuco, Peru

Deyvis Cano[1*], Mylee Príncipe[1], Debora Santa Cruz[1], Edu Albornoz[1], Loydith Benites[1], Niler Chahua-García[1], Julio Ángeles Suazo[2]

[1] Programa Académico de Ingeniería Ambiental, Universidad de Huánuco, Huánuco, Perú
[2] Escuela Profesional de Ingeniería Forestal y Ambiental, Universidad Nacional Autónoma de Tayacaja Daniel Hernández Morillo, Tayacaja, Perú
* Corresponding author's e-mail: deyvis.cano@udh.edu.pe

ABSTRACT

Atmospheric sedimentable dust (ASD) pollution is a critical environmental problem in urban and peri-urban areas. This study evaluated the spatiotemporal dynamics of ASD and its relationship with vehicular flow and meteorology along the Jancao–La Esperanza Road corridor (Huánuco). During 31 consecutive days, 10 sampling stations were monitored using the passive gravimetric method. Categorized vehicular flow was recorded through video surveillance, and meteorological variables were obtained from SENAMHI. The analysis integrated Spearman correlations, a lognormal generalized linear mixed model (GLMM), spatial IDW interpolation, and wind rose analysis. The highest cumulative daily deposition rate along the section occurred on May 17 (247.64 mg/cm²). The observational design, GLMM, and Spearman correlations demonstrated no statistically significant associations between the ASD deposition rate and fluctuations in vehicular flow or meteorological variables. Spatial variability among stations was negligible, whereas the sampling date explained the temporal fluctuations in the data. At the local level, station S-010 (northern sector) recorded the highest cumulative load (166.00 mg/cm²) and a daily median of 0.80 mg/cm²/day, associated with passive advection by NE–ENE winds and microlocal interception dynamics. It is concluded that ASD acts as background pollution governed by regional atmospheric dynamics rather than by local vehicular flow. This study provides unprecedented technical evidence for characterizing ASD deposition in inter-Andean valleys, offering a high-temporal-resolution monitoring scheme applicable to air quality management in peri-urban areas.

Keywords: air quality, wind dispersion, gravimetry, particulate matter, vehicular traffic.

INTRODUCTION

Atmospheric sedimentable dust (ASD) represents a relevant problem for air quality in urban and peri-urban areas. The growth of the vehicle fleet increases non-exhaust emissions associated with tire, brake, and pavement wear, as well as the resuspension of dust deposited on roads (Rodriguez et al., 2019; Harrison et al., 2021). Additionally, the internal combustion processes of vehicles emit pollutant gases that undergo chemical interactions in the atmosphere, serving as precursors to secondary particulate matter and fine aerosols (Cano et al., 2025). Vehicular traffic may mobilize previously deposited particles and alter their spatial and temporal distributions, particularly in areas with high traffic intensity (Alshetty and Nagendra, 2022; Zhang et al., 2024). This dynamic constitutes a factor of interest for air quality and population exposure to atmospheric particles (OMS, 2021).

ASD corresponds to the fraction of particles that, after remaining suspended, returns to surfaces through dry deposition processes. Its behavior depends on the physical properties of the particles and meteorological conditions, such as wind speed and relative humidity, which influence their transport, dispersion, and sedimentation (Farmer et al., 2021; Mallios et al., 2020). In this context, it is relevant to consider that the particulate matter load comprises not only resuspended dust but also contributions from vehicular combustion processes and atmospheric chemical transformations that promote the formation and accumulation of secondary particles from different sources (Cano et al., 2025). In turn, road dust constitutes a dynamic reservoir, generated, among other processes, by the wear of vehicular components and abrasion of the road surface. Its resuspension is conditioned by traffic-generated turbulence and environmental conditions (Khan et al., 2023). Therefore, vehicular intensity does not by itself determine the ASD deposition rate, since meteorological and surface factors simultaneously intervene.

Several studies have evaluated the influence of traffic and road conditions on the generation and distribution of ASD. Mendoza Atahuachi et al. (2025) reported that the deposition of pollutants in road environments responds to the interaction between traffic intensity and the physical characteristics of the terrain, whereas Miranda Casapia et al. (2019) and Álvarez-Tolentino and Suárez-Salas (2020) related the accumulation and resuspension of particles to vehicle density and pavement conditions. However, the magnitude of these relationships may vary among urban contexts due to differences in dust sources, road characteristics, meteorology, and mobility patterns.

In the city of Huánuco, urban expansion and increased vehicular traffic on connecting roads have created favorable conditions for the accumulation and resuspension of ASD, particularly along the Jancao–La Esperanza section, where areas with insufficient paving persist (Espinoza Mallqui, 2025; Amato et al., 2014a). Despite this, the available information on ASD behavior and its relationship with vehicular flow intensity in this area is limited. This lack of local evidence limits understanding of particle deposition dynamics in a territory undergoing urban expansion and increasing vehicular mobility.

In this context, the present study aimed to determine the temporal relationships among the ASD deposition rate, vehicular flow intensity, and meteorological factors along the Jancao–La Esperanza section in Amarilis, Huánuco. It also aimed to conduct an exploratory analysis of spatial patterns by IDW-interpolating ASD distribution in relation to wind direction during the monitoring period. Unlike the traditional literature focused on coastal environments or mining sites, this research provides the first comprehensive assessment of ASD in an inter-Andean peri-urban corridor. The novelty of the study lies in analyzing dust deposition dynamics using continuous 24-hour vehicular counts and local meteorological variables in a complex, understudied environment. The results aim to provide local evidence on the temporal and spatial dynamics of ASD and to establish a baseline that supports air quality monitoring and management in the study area.

MATERIALS AND METHODS

Study area

The study was conducted along the section between Jancao and La Esperanza, in the district of Amarilis, province and department of Huánuco, Peru. The section is connected to the city of Huánuco by an approximately 2 km paved road (Figure 1), of which the last 2 km were selected for the study. The mean annual temperature of this location is 20.38 °C, and the mean annual precipitation ranges from 387 to 403 mm, concentrated mainly between October and March, and to a lesser extent from May to August (Servicio Nacional de Meteorología e Hidrología del Perú [SENAMHI], 2025). Likewise, this sector presents flat slopes ranging from 0° to 2° (CENEPRED, 2021). From a socioeconomic perspective, the district of Amarilis had 85,304 inhabitants in the 2017 National Census, of whom 93.71% lived in the urban area and 6.29% in the rural area (Instituto Nacional de Estadística e Informática [INEI], 2017). In the district's urban area, commerce is reported as the main activity, followed by services (Garay et al., 2020). These characteristics describe the section as an area with a population, local traffic, and urban activities associated with daily mobility, constituting an important urban-peri-urban road corridor within the city (De Silva et al., 2024).

Field data sources

ASD sampling

ASD monitoring was conducted using the passive gravimetric method (Santillán-Lima

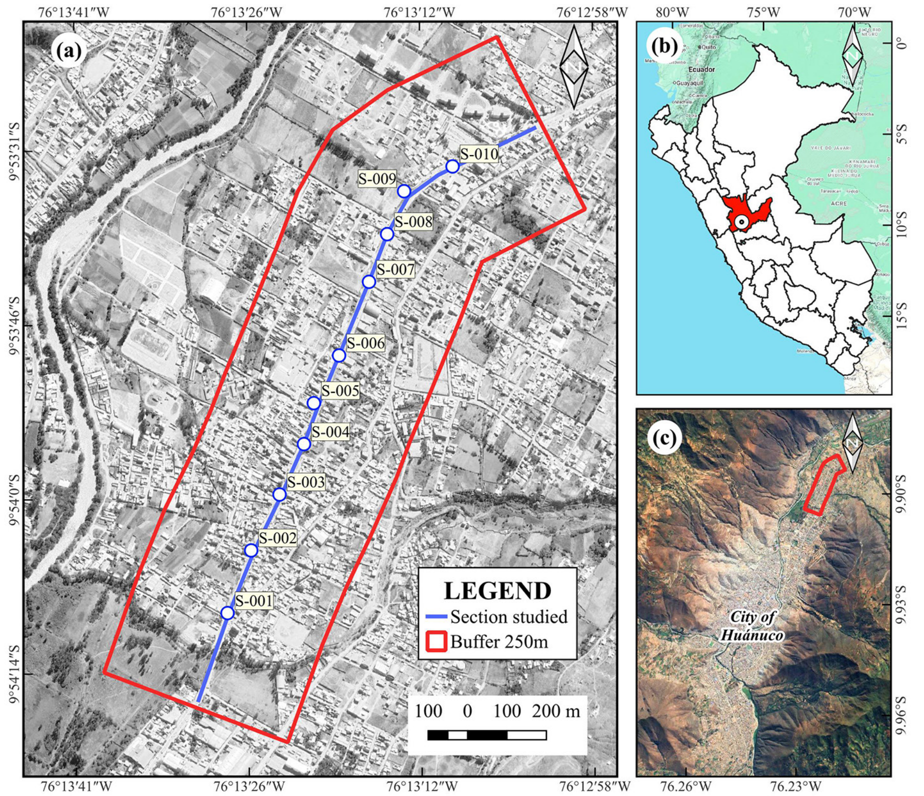

Figure 1. Delimitation of the study area and distribution of the monitoring points along the section between Jancao and La Esperanza, Amarilis (a), in the department of Huánuco (b), north of the city of Huánuco (c),. The spatial extent of the area was generated from a 250 m buffer around the studied section

et al., 2023) over a continuous 31-day period (May 7 to June 6). Ten georeferenced sampling stations (S-001 to S-010) were established and distributed between Jancao and La Esperanza, selected according to vehicular intensity, road proximity, urban coverage, and prevailing wind direction. As collectors, 100-mm-diameter glass Petri dishes (effective area of 78.54 cm²) were used, coded, and impregnated with a uniform film of neutral petroleum jelly as the collecting medium (Lazo Ramos et al., 2022). The dishes were installed in protective enclosures at a constant height of 3.30 m in 24-h exposure cycles. At the end of each cycle, the samples were removed, sealed, and transported to the laboratory for gravimetric quantification of the deposited mass. The determination of the initial mass and final mass was performed under controlled environmental conditions using two analytical balances with equivalent resolution (0.0001 g): A&D GR-200 (capacity: 210 g) and Sartorius Entris 124-1S (capacity: 120 g). Metrological equivalence between the instruments was ensured through leveling, daily zero adjustment, and verification with traceable standard weights prior to each session. The maximum estimated combined uncertainty was ±0.0002 g (±0.2 mg), a margin that does not compromise the accuracy of the calculated deposition rates.

Vehicular flow measurement

Vehicular flow was continuously recorded using an A9 HD IP camera (2 MP, 1920 × 1080 px) mounted at a height of 3.35 m with a 75° field of view at station S-010. Although the initial design contemplated traffic counts at both ends of the section (S-001 and S-010), the theft of equipment at S-001 early in the experiment limited measurements to S-010. Since the corridor extends 2 km without major intersections or significant detours, the count at S-010 was used as a proxy for the daily temporal variation in macro-vehicular volume at the corridor scale to evaluate its relationship with ASD deposition, recognizing that it does not describe microlocal fluctuations at the 10 stations.

The recordings covered 24 continuous hours (00:00 to 23:59 h) under different lighting conditions (daylight, backlighting, twilight, and nighttime). Audiovisual processing was performed using an automated computer vision script developed in Python (using object detection and trajectory tracking algorithms with OpenCV), configured according to the vehicle classification criteria of the National Vehicle Regulations of the MTC (Peru) to classify six vehicle types: private cars, collective vehicles, motorcycle taxis, rural transport vehicles, tourism vehicles, and pick-ups (Lazo Ramos et al., 2022). To ensure the accuracy of the algorithmic counts, 10% of the recordings were audited by independent observers through manual recounting.

Meteorological data source

Meteorological data were obtained from SENAMHI (https://www.senamhi.gob.pe/servicios/?p=estaciones). The Huánuco meteorological station, located in the district of Huánuco, was used as a reference, with coordinates of latitude 9°56'16.08'' S, longitude 76°14'52.55'' W, and an elevation of 1,947 m a.s.l., approximately 4 km from the study site. The variables of temperature (T, °C), wind speed (WS, m/s), relative humidity (RH, %), wind direction, and precipitation (PPT, mm) corresponding to the study monitoring period (May 7 to June 6, 2026) were collected. These variables were considered to characterize the environmental conditions associated with the dispersion, transport, and deposition of atmospheric sedimentable dust during the monitoring period.

Data processing

ASD data

The ASD records were organized by monitoring point code, UTM coordinates, elevation, installation date, collection date, plate code, exposure days, collection area, and the initial and final weights of the exposed plate. Using this data, the accumulated deposited mass was calculated as the difference between the final and initial weight of the plate conditioned with petroleum jelly. The ASD deposition rate was calculated using the gravimetric method and expressed in mg/cm²/day. For this purpose, the following equation was used:

$$ASD = \left[\frac{(Pf - Pi) \times 1000}{A \times t}\right] \quad (1)$$

where: *ASD* – deposition rate, in mg/cm²/day; *Pf* – final weight of the exposed plate, in grams (g); *Pi* – initial weight of the plate conditioned with petroleum jelly, in grams (g); 1000 – conversion factor from grams (g) to milligrams (mg); *A* – collection area of the plate, in cm²; *t* – exposure time, in days.

The collection area corresponds to the exposed surface of the Petri dish on which sedimentable particles are deposited during the monitoring period and is assumed to be a standard area for all samples, at 78.54 cm². Since the dish has a circular shape, the area was determined using the equation for the area of a circle:

$$A = \pi \times r^2 \quad (2)$$

where: *A* – collection area (in cm²); *π* – constant 3.1416; *r* – radius of the Petri dish (in cm).

The primary data corresponding to the 310 gravimetric observations (Pi, Pf, area, exposure time, and calculated deposition rates) are available in Data S1 of the Supplementary Dataset.

Spatial interpolation analysis

To characterize the continuous spatial patterns of ASD along the section, daily interpolation was performed using the inverse distance weighting (IDW) method in QGIS (v. 3.40.15), generating raster surfaces with a spatial resolution of 2 m. The 31-day time series was summarized at the cell level using three robust metrics to mitigate the effects of outliers: total accumulated deposition, daily median (representative of the continuous baseline level), and interquartile range (IQR, an indicator of localized temporal variability).

To evaluate the accuracy of the generated surfaces, leave-one-out cross-validation (LOOCV) was applied. The resulting errors indicated high spatial uncertainty among stations, derived from the available sampling density. Consequently, the interpolated maps are used strictly for exploratory and qualitative purposes to illustrate general trends along the road corridor and are not used for causal inference or regulatory zoning.

Vehicular flow data

The vehicular traffic count data were reviewed and organized into an hourly matrix, considering the recording date, hourly interval, counting point, and vehicle category, in accordance with the Ministry of Transport and Communications (Table 1). Subsequently, the hourly records from 00:00 to 23:59 h were summed to obtain the daily vehicular flow for each category and the total daily vehicular flow.

This transformation enabled the identification of daily traffic variation during the monitoring period and the generation of a database compatible with the daily ASD records for subsequent integration and joint analysis. In cases of incomplete records, these were identified and excluded from the corresponding daily analysis to avoid bias in estimating total vehicular flow. The vehicular count was initially recorded in four categories: light vehicles, passenger transportation, freight, and trailers. In order to avoid multicollinearity among the heavy-duty subcategories and to more stably reflect the resuspension load, these variables were consolidated for modeling into two functional groups: (1) Light Vehicles and (2) Heavy Vehicles. The consolidated hourly matrix of vehicle counts by category throughout the entire monitoring period is presented in Data S2 of the Supplementary Dataset.

Meteorological data

The meteorological records were organized chronologically and transformed to a daily scale. For air temperature, relative humidity, and wind speed, daily averages were calculated; for precipitation, 24-h accumulated values were calculated; and for wind direction, the predominant direction according to its daily frequency was determined. The distribution of wind direction and speed was visualized using WRPLOT. Finally, the daily ASD data, vehicular flow, and meteorological variables were integrated into a common date-based matrix to evaluate their relationships during the monitoring period.

Statistical data analysis

Descriptive statistics were used to characterize and represent the ASD deposition rate, vehicular flow, and meteorological variables. Preliminary bivariate associations were evaluated using the Spearman correlation coefficient (rho). Meteorological and traffic variables were aggregated into daily intervals coinciding with the 24-h exposure window of the ASD collectors (Lag 0). This contemporary approach was prioritized to account for the temporal resolution of passive gravimetric sampling and to preserve the statistical power of the observational time series ($N = 31$ independent days).

To evaluate the influence of meteorological and vehicular predictors on ASD deposition ($N = 310$ observations), a Generalized Linear Mixed Model (GLMM) with a Log-Normal distribution and logarithmic link function was fitted using the glmmTMB package in R. The response variable (ASD, expressed in $mg/cm^2/day$) was entered on its original scale ($Y > 0$), allowing the Log-Normal family to directly model the positive skewness of the data. Continuous predictor variables (temperature, relative humidity, wind speed, heavy traffic, and light traffic) were standardized (z-score: mean = 0, SD = 1) to homogenize their scales and facilitate comparison of the magnitude of their regression coefficients (β). Precipitation was included as a

Table 1. Official vehicle classification – Directive No. 002-2006-MTC/15

Official MTC category	Specific subclass	Actual description of vehicle type on the road section
Category L (Light vehicles)	L3	Two-wheeled motorcycles.
Category L (Light vehicles)	L5	Passenger three-wheeled vehicles (motorcycle taxis). The most abundant vehicle on the road.
Category M (Passenger vehicles)	M1	Private automobiles, station wagons, and sedans (collective transportation service).
Category M (Passenger vehicles)	M2	Minibusses/vans (interurban public transportation Huánuco–Jancao–La Esperanza).
Category M (Passenger vehicles)	M3	Large urban and interprovincial buses.
Category N (Freight vehicles)	N1	Pick-up trucks, light distribution and delivery vans.
Category N (Freight vehicles)	N2	Medium-sized two-axle trucks, flatbed trucks, and medium dump trucks (GVW between 3.5 t and 12 t).
Category N (Freight vehicles)	N3	Heavy trucks and 3- to 4-axle dump trucks (GVW greater than 12 t).
Category O (Trailers)	O3 / O4	Semitrailers and heavy trailers attached to articulated trucks.

binary categorical variable (Precipitation: Yes/No). To control for structural autocorrelation arising from repeated measurements, crossed random effects by monitoring station (u_i, spatial variability) and sampling date (v_j, temporal variability) were specified.

The formal structure of the Log-Normal GLMM is defined as:

$$\ln(\mathrm{ASD}_{ij}) = \beta_0 + \beta_1 z_{\mathrm{Temp},j} + \beta_2 z_{\mathrm{Hum},j} + \\ + \beta_3 z_{\mathrm{Wind},j} + \beta_4 \mathrm{Precip.}_j + \beta_5 z_{\mathrm{Heavy\ t.},j} + \\ + \beta_6 z_{\mathrm{Light\ t},j} + u_i + v_j + \varepsilon_{ij} \quad (3)$$

where: ASD_{ij} represents the observed deposition rate at station i (i = 1,..., 10) during day j (j = 1,..., 31); β_0 is the intercept; $\beta_1 \ldots \beta_6$ are the regression coefficients of the fixed effects; $u_i \sim \mathcal{N}(0, \sigma^2_{\mathrm{Station}})$ is the spatial random effect by station; $v_j \sim \mathcal{N}(0, \sigma^2_{\mathrm{date}})$ is the temporal random effect by date; and $\varepsilon_{ij} \sim \mathcal{N}(0, \sigma^2_e)$ represents the random residual.

The selection of the distribution family for the generalized linear mixed model (GLMM) was evaluated by comparing the Log-normal specification against the alternative Gaussian (conventional LMM) and Gamma (log link) models, keeping the fixed and random effects structure (1 | Station) + (1 | Date) constant, a decision based on the characterization of the original variable (skewness and Shapiro-Wilk normality test), likelihood (log L), and the Akaike (AIC) and Bayesian (BIC) Information Criteria. The validation of assumptions and the analytical behavior of the models were evaluated using simulated quantile residuals with the DHARMa package (Kolmogorov-Smirnov, dispersion, and outlier detection tests), and the significance of fixed effects was determined using Type III Wald tests (χ^2). Additionally, two parallel sensitivity analyses were performed: on one hand, coefficient stability against extreme events was evaluated by refitting the GLMM after excluding observations above the 95th percentile; on the other hand, to rule out bias due to spatial pseudoreplication or random effects specification stemming from the use of constant daily predictors across the ten stations, a multiple linear regression was fitted on the log-transformed daily transect mean ($\ln\mathrm{ASD}_{\mathrm{mean}}$) considering N = 31 independent days.

RESULTS

Temporal variations in ASD and vehicular flow intensity

The daily ASD deposition rate showed marked fluctuations during the monitoring period, with the highest peaks occurring between May 16 and 20, 2026, at all stations (Figure 2a). The maximum value occurred on May 17, with a total deposition rate across the 10 stations of 247.64 mg/cm²/day, driven mainly by station S-010. This event was followed by peaks on May 20 (173.75 mg/cm²/day) and May 19 (141.55 mg/cm²/day), supported by contributions from stations S-002 and S-003. The minimum deposition rates were observed on May 15 and 23, with daily accumulated values of 2.33 and 2.68 mg/cm²/day, respectively. At the station level during the 31-day study period, station S-010 recorded the highest load, with a total accumulation of 166.00 mg/cm² and a daily median of 0.80 mg/cm²/day. In contrast, station S-009 recorded the lowest levels along the section, with a total accumulation of 87.81 mg/cm² and a daily median of 0.56 mg/cm²/day. It should be emphasized that while the peak on May 20 was indeed due to S-002 and S-003, the event on May 19 resulted from a generalized, simultaneous increase at most of the other stations (S-001, S-004, S-005, S-006, and S-008).

The distribution of ASD evidenced a continuous spatial baseline level along the section (Figure 2b; data transformed to log (ASD + 1) exclusively for graphical visualization purposes and not for statistical analysis). Daily medians remained consistent among the monitoring points, ranging from 0.42 to 1.21 mg/cm²/day. Higher outlier values were recorded at stations S-001, S-002, S-003, S-007, and, with greater magnitude, at S-010 (exceeding 28.33 mg/cm²/day during isolated events). Spatial variability among the 10 monitoring stations was evaluated through the variance component of the random intercept by station (1 | Station) in the GLMM, obtaining an estimated variance close to zero ($\sigma^2_{\mathrm{station}}$ = 4.388 × 10^{-10}). This indicates that the ASD deposition rate remained relatively uniform along the evaluated section, with no significant spatial differences among the sampling points after adjusting for the daily effect.

Vehicular flow exhibited distinct temporal patterns by functional category (Figure 3a). Passenger transport vehicles (M1/M2/M3) recorded the highest volumes along the section, peaking at 5,191 vehicles/day on May 18 and falling to 1,639 vehicles/day on May 9, 2026, with systematic declines on weekends. In contrast, the light vehicle fleet (L3/L5) showed the greatest temporal stability throughout the monitoring period, remaining within a constant range of 2685 to 3217 vehicles/day, without reductions on Saturdays and Sundays. The freight vehicle (N1/N2/N3) and trailer (O3/O4) categories presented lower flows, recording daily ranges of 321–801 vehicles/day and 0–57 vehicles/day, respectively, with an almost complete reduction in trailer traffic during weekends (0–4 vehicles/day).

Meanwhile, the meteorological variables, with values transformed for visual purposes (standardized: temperature, relative humidity, wind speed; logarithmic: precipitation), showed marked temporal covariation during the evaluation campaign (Figure 3b). Although climatic fluctuations did not show a direct correspondence with the episodic peaks in ASD deposition, specific modulations in the time series were identified. In particular, on days with recorded precipitation (May 11, 12, and 21), standardized relative humidity increased significantly, peaking on May 21, accompanied by decreases in temperature and wind speed.

Relationship of ASD with meteorological variables and vehicular flow

The multiple Spearman correlation analysis (Figure 4) confirmed that the individual bivariate associations between ASD and the predictors were weak and non-significant $p < 0.05$): temperature (r_s =0.03), humidity (r_s =0.08), wind speed (r_s =-0.09), precipitation (r_s =0.04), light vehicles (r_s =0.06), and passenger transport (r_s =0.07). These results justified the subsequent use of GLMM with random effects to capture multivariate temporal variability.

The generalized linear mixed model (GLMM) with a Log-Normal distribution and

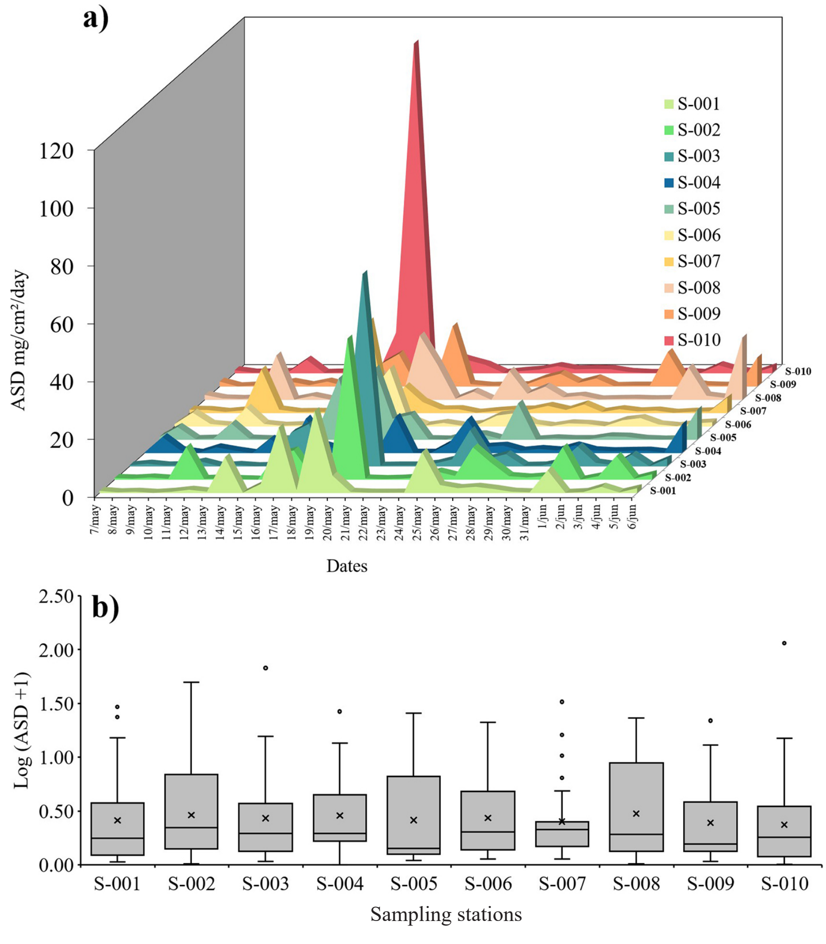

Figure 2. Daily temporal variation in the ASD deposition rate during the monitoring period (a). Boxplot distribution of the ASD deposition rate across all stations with log (ASD + 1) transformation (b)

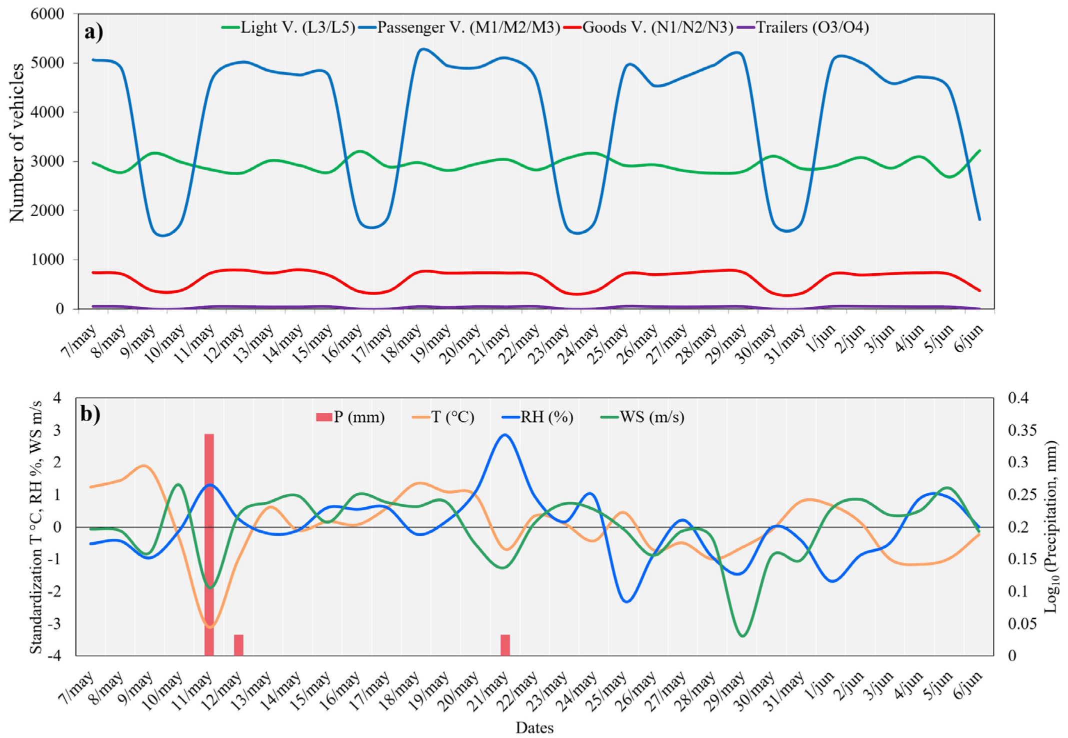

Figure 3. Daily time series of vehicular traffic conditions and meteorological variables recorded during the monitoring period: (a) daily vehicular volume categorized by vehicle type, (b) temporal dynamics of the transformed meteorological variables

Type III Wald test confirmed that no meteorological or vehicular predictor significantly affected the ASD deposition rate (p > 0.60 in all cases; Table 2). Consequently, no statistically significant associations were detected between the variables evaluated and ASD during the study period. This finding indicates that ASD does not act as a primary pollutant that disperses immediately in response to local vehicular flow, but rather as regional background pollution. The model intercept was highly significant ($\beta = 1.220$, SE = 0.140, $\chi^2 = 75.42$, $p < 0.001$), representing an estimated baseline deposition rate of 3.39 mg/cm²/*day* [exp(1.220)]; that is, the expected average load when continuous variables are at their mean values and in the absence of rainfall.

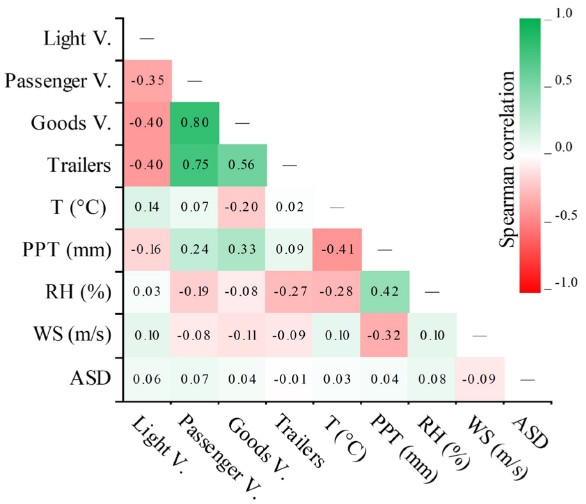

Figure 4. Bivariate spearman correlation matrix analysis

The random-effects structure showed that spatial variability among stations was practically null ($\sigma^2_{station} = 4.388 \times 10^{-10}$), whereas temporal variability by sampling date explained most of the dispersion ($\sigma^2_{Date} = 0.2811$). This difference confirms that ASD deposition is spatially homogeneous throughout the section and that its dynamics respond to atmospheric processes at the macro scale. Finally, simulated residual diagnostics using the DHARMa package (Figure 5) confirmed the absence of overdispersion (dispersion test: p = 0.392) and severe outliers (dispersion test: p = 0.741). Although the Kolmogorov–Smirnov test detected a deviation from residual uniformity (KS test: p = 0.00051), this is attributable to the presence of the acute episodic events recorded in mid-May, without altering the robustness of the estimates or the absence of effects from the evaluated predictors.

Table 2. Fixed effects results of the log-normal GLMM for ASD and Type III Wald Test

Predictor variable	Estimate (β)	Standard error (SE)	z-value	Chi-square (χ^2)	Degrees of freedom (df)	p-value	Significance
(Intercept)	1.220	0.140	8.684	75.416	1	< 0.001	***
Temperature (standardized)	0.008	0.123	0.063	0.004	1	0.950	n.s.
Humidity (standardized)	0.028	0.128	0.221	0.049	1	0.825	n.s.
Wind (standardized)	-0.059	0.113	-0.518	0.269	1	0.604	n.s.
Rain (category: Yes/No)	0.007	0.496	0.014	0.0002	1	0.989	n.s.
Heavy vehicles (standardized)	-0.027	0.129	-0.212	0.045	1	0.832	n.s.
Light vehicles (standardized)	0.064	0.128	0.498	0.248	1	0.619	n.s.
Random effects							
Groups		Variance		Standard deviation			
Station (10 points)		$\sigma^2 = 4.388 \times 10^{-10}$		$\sigma = 2.095 \times 10^{-5}$			
Date (31 days)		$\sigma^2 = 0.2811$		$\sigma = 0.5302$			
Model fit metrics							
Metric		Value					
Sample (N) / residual df		310 / 300					
AIC / BIC		1134.3 / 1171.6					
Deviance / Dispersion		1114.3 / 8.97					

Model comparison and sensitivity analysis

Comparison of distributional families showed that, although the Gamma model had a lower AIC (AIC = 1115.80) than the Log-Normal model (AIC = 1134.3), residual diagnostics using DHARMa revealed significant deviations from the assumptions of the Gamma distribution ($p = 0.00119$ in the KS test; Figure S5a). In contrast, the Log-Normal model showed the best overall fit and stability in the dispersion and outlier tests (dispersion test: $p = 0.392$; outlier test: $p = 0.741$; Figure S5b and Table S5), making it the most inferentially robust model for the analysis.

To justify the use of the model, it was found that the ASD deposition rate on its original scale exhibited marked positive skewness (skewness coefficient = 7.15) and a severe deviation from

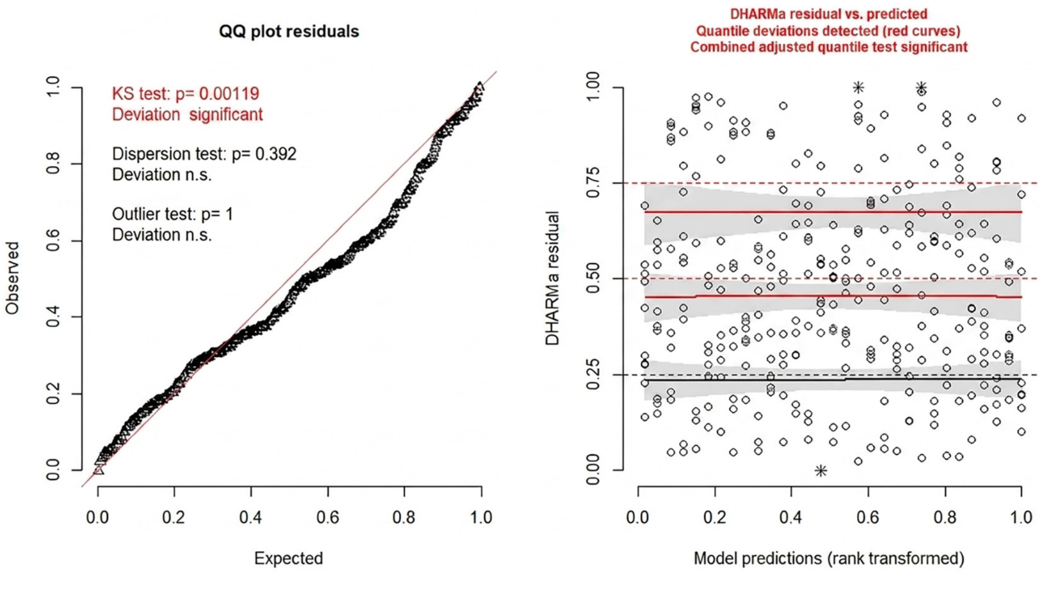

Figure 5. DHARMa simulated residual diagnostics for the fitted model

normality (Shapiro-Wilk test: $W = 0.389$, $p < 0.001$), confirming the inadequacy of the traditional Gaussian model ($\log L = -1101.97$; AIC = 2223.93). When evaluating alternative families for positively skewed continuous data, the Gamma distribution presented a lower AIC (AIC = 1115.80; $\log L = -548.90$) than the Log-Normal specification (AIC = 1134.37; $\log L = -558.19$). However, diagnostic inspection of simulated quantile residuals revealed a statistically significant deviation from theoretical assumptions in the Gamma model ($p = 0.0019$ in the KS test; Table S2 and Figure S1a). Conversely, the Log-Normal model guaranteed the best overall fit and structural stability, satisfying the assumptions of homoscedasticity and uniformity in the residual distribution ($p = 0.2423$ in the KS test; Table S2 and Figure S1b), thereby constituting the inferentially most robust structure for analysis.

The sensitivity analysis at the independent daily level ($N = 31$) confirmed the stability of the findings from the main analysis: no meteorological or traffic predictor reached statistical significance ($p > 0.05$ across all covariates) (Table S1). The invariance in the absence of significant effects between the daily-disaggregated and daily-aggregated scales supports the primary model, demonstrating that the findings are robust and not biased by the random effects structure.

Likewise, the sensitivity analysis performed after excluding the outlier values (N = 294) confirmed that no meteorological variable or vehicle category significantly influenced the ASD deposition rate ($p > 0.05$ in all cases; Table S5). This result demonstrates that the lack of significance in the main model reflects the actual dynamics of pollution and does not reflect a statistical artifact from episodic peak events or extreme values.

Spatial distribution of ASD deposition and wind dynamics

The exploratory spatial analysis using IDW interpolation showed descriptive spatial gradients in ASD deposition across the study area (Figure 6). The interpolated surfaces represent continuous approximations of the deposition rate per cell. The monthly accumulation (Figure 6a) identified the highest ASD load at stations S-010 (northeastern end), S-002, and S-003 (southern sector). The median deposition rate (Figure 6b) exhibited consistently low values throughout the section (≤ 1.1 to 1.8 mg/cm^2/day), reflecting a relatively stable spatial baseline level. In contrast, the variability expressed by the IQR (Figure 6c) showed marked spatial fluctuations, with the highest values (>4.4 mg/cm^2/day) located at stations S-008 (northern sector) and S-002/S-005 (southern sector). These points of high variability coincide with the greatest total accumulation recorded during the monitoring period (Figure 6a; >134.9 mg/cm^2/day), indicating that total accumulation in these sectors is driven by discrete episodic resuspension events rather than by a constant elevation of the baseline. The anemometric analysis (Figure 6d) identified a dominant wind flow originating from the Northeast sector (NE–ENE), reaching gusts of up to 8.8 m/s in 12.6% of the observations (with 7.02% of calm periods), which coincides with the orientation of the road section and suggests a preferential vector for the wind-driven transport of sedimentable particles.

DISCUSSION

The Type III Wald test of the GLMM and Spearman correlations detected no statistically significant associations between vehicle traffic intensity and daily ASD deposition ($p > 0.05$). This lack of statistical significance does not prove the absence of a physical resuspension effect, but rather indicates that, given the sample's statistical power and temporal resolution (N = 31 days), daily traffic variability did not detectably explain the deposition rate in the collectors. These findings differ from those reported by Delgado Alvarado (2019) in Trujillo and by Mayta-Merma et al. (2021) in Ilave (Puno), where higher volumes of vehicular traffic directly and proportionally increased the concentration of sedimentable dust on roadways. However, they are consistent with the findings reported by Lazo Ramos et al. (2022) along Av. Cusco Road corridor in Tacna, who also did not identify a significant correlation between urban transportation flow and particle levels captured through passive sampling (Rho = -0.153, $p > 0.05$). Cross-contextual discrepancies suggest that the relationship between traffic flow and ASD is neither linear nor direct, but rather strongly mediated by vehicle speed, local sediment availability, and road surface condition. Therefore, ASD along this road segment statistically behaved like background pollution, with daily fluctuations not coupled to recordable traffic volume.

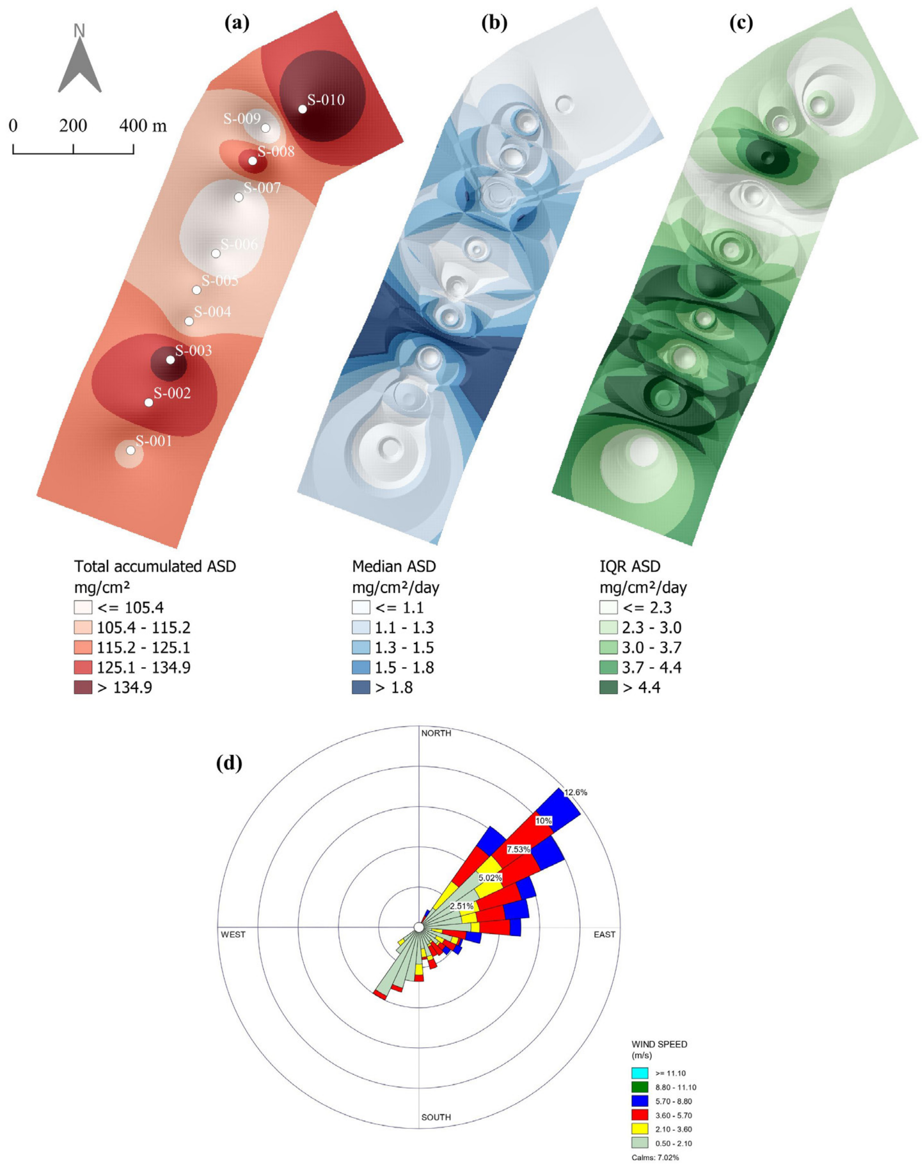

Figure 6. Exploratory spatial patterns of ASD deposition during the 31-day monitoring period: (a) total accumulated deposition during the study period (mg/cm^2), (b) daily median deposition rate (mg/cm^2/day), (c) Interquartile range (mg/cm^2/day), (d) wind rose illustrating the prevailing wind speed and direction during the study

Similarly, the absence of significant associations with meteorological predictors ($p > 0.05$) reflects the limitations of the observational design to capture contemporaneous linear relationships during a short dry period, and should not be interpreted as an absence of meteorological control over particle dynamics. This behavior contrasts directly with the research conducted by Chávez Pérez (2018) in the urban area of Huánuco, where climate (temperature, wind speed, and precipitation) had an inverse and decisive effect on the deposition of sedimentable particles. Similarly, it differs from the findings reported by Enciso Tuanama (2023) in Yarinacocha (Ucayali), who documented that precipitation and relative humidity exerted decisive natural control over dust deposition, with strong negative correlations with ASD (p = 0.000). However, the contemporary findings of this study are consistent with the climatic homogeneity and low meteorological sensitivity described by García Chirinos (2024) on paved avenues in Huancayo. In this scenario, macroscale wind dynamics serve as the primary vector for regional transport, while surface microclimatic variations do not reach a sufficient magnitude to generate statistically detectable responses at the evaluated daily scale. (Farmer et al., 2021).

The variance decomposition of the multivariate mixed model revealed that the net spatial variability among the 10 monitoring stations along the 2 km section was statistically null ($\sigma^2_{station} = 4.388\times10^{-10}$), with daily temporal variation (daily temporal variation) explaining the entirety of the data dispersion. Although Cartesian geostatistical interpolation (IDW) suggests local visual gradients along the peri-urban corridor, the GLMM's statistical inference reconfirms the spatial homogeneity of the central tendency once daily variability is accounted for. This apparent divergence between the continuous visualization of raster maps and the inferential rigor of the mixed model differs from the behavior documented by Santillán-Lima et al. (2023) in Cajabamba (Ecuador) and by Chambilla Tello et al. (2024) on the university campus of Tacna; in both studies, geostatistical modeling (Kriging and IDW, respectively) captured and validated marked spatial differences (hotspots) generated by the direct proximity of highly specific fixed anthropogenic sources (such as concrete block factories or grain mills). Regarding the anomalous behavior, the episodic deposition peaks qualitatively recorded at station S-010 (northern sector of the section), the wind rose, and the orientation of the section lead to the exploratory hypothesis that local dry deposition dynamics may be modulated by fine-scale micrometeorological variations, immediate terrain roughness, and artificial physical barriers that locally alter wind energy and favor mechanical sedimentation by gravity (Csavina et al., 2012; Amato et al., 2014b). Nevertheless, given the available sampling density (N = 10) and the uncertainty inherent in the LOOCV validation of the IDW method, station S-010 should be interpreted with academic caution, not as a definitive pollution hotspot, but as a focal area of interest for future investigations with denser microscale sampling.

The study presents methodological limitations that should be acknowledged. First, the 31-day monitoring window does not encompass seasonal or interannual variability in the area. Second, logistical constraints limited automated vehicular counting to a single counting point at the corridor scale (2 km) and placed the reference meteorological station 4 km from the study site, which prevented the capture of micro-vehicular variations (such as acceleration or congestion in front of each collector) or high-resolution microclimatic fluctuations. Third, the model evaluated only the contemporaneous relationship (Lag 0); given that physical processes such as sediment drying and resuspension may exhibit 24- to 48-hour inertia (Lag 1 or Lag 2), future studies with continuous high-frequency monitoring will allow delayed effects to be evaluated. Finally, the lack of chemical speciation prevented precise analytical attribution of emission sources. Despite these limitations, the diagnostic robustness of the Log-Normal GLMM, the methodological design, and the assessment of traffic dynamics provide a much more rigorous and representative characterization of vehicular impacts. This ensures the reliability of the inferences and provides an empirical baseline for environmental management and road maintenance in urban and peri-urban corridors.

CONCLUSIONS

Under the observational design and the evaluated monitoring window (N = 31 independent days), the GLMM detected no statistically significant associations ($p > 0.05$) between traffic flow fluctuations or meteorological variables and the ASD deposition rate. This result indicates that, given the available temporal resolution and sample size, daily ASD variations showed no direct coupling with short-term changes in local traffic or surface weather, statistically behaving as a constant background environmental load governed by inter-day temporal dynamics that reached their highest accumulation on May 17 (247.64 mg/cm^2/day). Although the spatial random variance between stations was practically zero ($\sigma^2_{\text{Station}} \approx 0$), cartographic exploration revealed episodic accumulations in the northern sector (station P-010), potentially modulated by passive advection attributable to prevailing NE–ENE winds.

From an environmental management perspective, failing to detect a direct proportional relationship between traffic volume and daily deposition during this period suggests that traffic acts predominantly as a physical resuspension agent on a pre-existing reservoir rather than as the primary source of the daily deposited mass. Consequently, mitigation strategies should not be limited to traffic volume control but should prioritize reducing road sediment load through scheduled watering, mechanical sweeping, and unpaved surface stabilization in the northern sector. Since the absence of statistical significance does not equate to the non-existence of physical impact, future research is recommended to expand the monitoring window to seasonal scales, increase sampling frequency to evaluate potential lagged effects, and incorporate chemical speciation analysis for analytical source apportionment.

Acknowledgments

The authors thank engineer Jorge Romero for his advice on the methodology; engineer Albert Soto for guidance on the literature review; and engineers Hernán Atilio and Gisela Lázaro for access to and use of materials from the Environmental Chemistry Laboratory of the Universidad de Huánuco.

REFERENCES

1. Alshetty, D., Nagendra, S. M. S. (2022). Impact of vehicular movement on road dust resuspension and spatiotemporal distribution of particulate matter during construction activities. *Atmospheric Pollution Research, 13*(1), 101256. https://doi.org/10.1016/J.APR.2021.101256
2. Álvarez-Tolentino, D., Suárez-Salas, L. (2020). Aporte cuantitativo de las fuentes de PM10 y PM2.5 en sitios urbanos del Valle Del Mantaro, Perú. *Revista Internacional de Contaminación Ambiental, 36*(4), 875–892. https://doi.org/10.20937/RICA.53473
3. Amato, F., Cassee, F. R., Denier van der Gon, H. A. C., Gehrig, R., Gustafsson, M., Hafner, W., Harrison, R. M., Jozwicka, M., Kelly, F. J., Moreno, T., Prevot, A. S. H., Schaap, M., Sunyer, J., Querol, X. (2014). Urban air quality: The challenge of traffic non-exhaust emissions. *Journal of Hazardous Materials, 275*, 31–36. https://doi.org/10.1016/J.JHAZMAT.2014.04.053
4. Amato, F., Karanasiou, A., Cordoba, P., Alastuey, A., Moreno, T., Lucarelli, F., Nava, S., Calzolai, G., Querol, X. (2014). Effects of road dust suppressants on PM levels in a Mediterranean urban area. *Environmental Science & Technology, 48*(14), 8069–8077. https://doi.org/10.1021/ES502496S
5. Cano, D., Peñaloza, R., Cacciuttolo, C., Kuplich, T. M., Ramírez, D. W., Suárez-Salas, L. (2025). Impact of the suspension of a metallurgical complex: SO2 analysis and vegetation restoration through remote sensing. *Advances in Meteorology, 2025*(1), 4732468. https://doi.org/10.1155/ADME/4732468
6. Centro Nacional de Estimación Prevención y Reducción de Riesgo de Desastres [CENEPRED]. (2021). Lineamientos para la elaboración del Informe de Evaluación del Riesgo de Desastres en Proyectos de Infraestructura Educativa. https://www.gob.pe/institucion/cenepred/informes-publicaciones/1867447-lineamientos-para-la-evaluacion-del-informe-de-evaluacion-del-riesgo-de-desastres-en-proyectos-de-infraestructura-educativa
7. Chambilla Tello, A. K., Mamani, A. Y. N., Cosi Mollinedo, L. J., Caceres Calisaya, A., Carita Ccosi, R. B. (2024). Modelamiento geoestadístico de la dispersión de polvo atmosférico sedimentable en puntos de influencia dentro del campus universitario en la ciudad de Tacna, Perú. *Sciencevolution, 4*(12), 201–211. https://doi.org/10.61325/SER.V4I12.145
8. Chávez Pérez, P. (2018). *Contaminación del aire por material particulado sedimentable en la zona urbana de Huánuco de agosto a octubre del 2016* [Undergraduate thesis, Universidad Nacional Agraria de la Selva]. https://hdl.handle.net/20.500.14292/1366
9. Csavina, J., Field, J., Taylor, M. P., Gao, S., Landázuri, A., Betterton, E. A., Sáez, A. E. (2012). A review on the importance of metals and metalloids in atmospheric dust and aerosol from mining operations. *Science of The Total Environment, 433*, 58–73. https://doi.org/10.1016/J.SCITOTENV.2012.06.013
10. de Silva, A., Ranasinghe, R., Sounthararajah, A., Haghighi, H., Kodikara, J. (2024). Beyond conventional monitoring: a semantic segmentation approach to quantifying traffic-induced dust on unsealed roads. *Sensors, 24*(2), 510. https://doi.org/10.3390/S24020510
11. Delgado Alvarado, J. L. (2019). *Influencia del flujo vehicular, en la contaminación por polvo atmosférico sedimentable en el mercado zonal Palermo - Trujillo, 2019* [Undergraduate thesis, Universidad César Vallejo]. In Repositorio Institucional - UCV. https://repositorio.ucv.edu.pe/handle/20.500.12692/48368
12. Enciso Tuanama, R. K. (2023). *Evaluación de Polvo Atmosférico Sedimentable (PAS) mediante muestreo pasivo en Yarinacocha, Ucayali 2022* [Undergraduate thesis, Universidad Peruana Unión]. https://hdl.handle.net/20.500.12840/6387
13. Espinoza Mallqui, M. E. (2025). *Evaluación de la concentración de dióxido de azufre (SO2) en el aire, generada por el parque automotor en el ingreso principal de la Universidad de Huánuco, distrito de Amarilis-2024* [Undergraduate thesis, Universidad de Huánuco]. In Universidad de Huánuco. https://repositorio.udh.edu.pe/handle/20.500.14257/5749
14. Farmer, D. K., Boedicker, E. K., Debolt, H. M. (2021). Dry deposition of atmospheric aerosols: approaches, observations, and mechanisms. *Annual Review of Physical Chemistry, 72*, 375–397. https://doi.org/10.1146/annurev-physchem-090519-034936
15. Garay Trujillo, D., Rodríguez Cruz, W., Valverde

Miraval, E. N. (2020). *Crecimiento comercial y su incidencia en la calidad de vida de los pobladores del centro poblado de la Esperanza, Amarilis, Huánuco, período 2018.* [Undergraduate Thesis, Universidad Nacional Hermilio Valdizán]. https://repositorio.unheval.edu.pe/item/d959d638-1afd-4a30-a5e0-284cf0a3a50e

16. Garcia Chirinos, L. F. (2024). *Evaluación y monitoreo de polvo atmosférico sedimentable en la vía pavimentada y no pavimentada de la avenida Ferrocarril en el distrito de El Tambo, provincia de Huancayo, mediante el método de placas receptoras* [Undergraduate thesis, Universidad Continental]. https://repositorio.continental.edu.pe/item/1e755b77-bb44-4e7b-bcae-ef8bfb2235cb
17. Harrison, R. M., Allan, J., Carruthers, D., Heal, M. R., Lewis, A. C., Marner, B., Murrells, T., Williams, A. (2021). Non-exhaust vehicle emissions of particulate matter and VOC from road traffic: A review. *Atmospheric Environment, 262*, 118592. https://doi.org/10.1016/J.ATMOSENV.2021.118592
18. Instituto Nacional de Estadística e Informática [INEI]. (2017). *Censos Nacionales 2017 – XII de Población, VII de Vivienda y III de Comunidades Indígenas*. https://censo2017.inei.gob.pe/
19. Jiang, W., He, C., Huang, Y., Wang, T., Yuan, D., Wu, W., Fan, H. (2025). Diffusion of re-suspended dust induced by vehicles: Full-scale simulation and field test. *Transportation Research Part D: Transport and Environment, 139*, 104552. https://doi.org/10.1016/J.TRD.2024.104552
20. Khan, S., Hassan, Q., Kumar, K., Dixit, S., Sharma, K., Vivek Kumar, C., Dhaliwal, N., Madhu, B. (2023). Modelling the Impact of Road Dust on Air Pollution: A Sustainable System Dynamics Approach. *E3S Web of Conferences, 430*, 01176. https://doi.org/10.1051/E3SCONF/202343001176
21. Lazo Ramos, R. S., Román Arce, R. C., Sisa Yataco, R. H., Mamani Vargas, R. B., Lanchipa Ugarte, S. E. (2022). Partículas suspendidas totales (PST) y flujo vehicular en una avenida de la ciudad de Tacna. *Ingeniería Investiga, 4*, 2022. https://doi.org/10.47796/ing.v4i0.656
22. Mallios, S. A., Drakaki, E., Amiridis, V. (2020). Effects of dust particle sphericity and orientation on their gravitational settling in the earth's atmosphere. *Journal of Aerosol Science, 150*, 105634. https://doi.org/10.1016/J.JAEROSCI.2020.105634
23. Mayta-Merma, W., Larico-Mamani, C. J., Fernandez-Mamani, D. L., Cahua-Alvarez, J. L., Cabana-Alanoca, R., Quiñonez-Choquecota, J. (2021). Concentración y dispersión de polvo sedimentable y material particulado PM10 a causa del trafico vehicular en periodo estiaje, en la zona del Cercado de la ciudad de Ilave. *Revista el Ceprosimad, 9*(1), 06–14. https://doi.org/10.56636/CEPROSIMAD.V9I1.100
24. Mendoza Atahuachi, M. A., Suricallo Menendez, P., Mamani, Y. A., Fabiana, N., Maquera, V., Stony, A., Zavala, G. (2025). Evaluación de la concentración de PAS y material particulado PM2.5 y PM10, Alto de la Alianza - 2025. *Ciencia y Educación, 6*(7.1), 90–98. https://doi.org/10.5281/ZENODO.16412959
25. Miranda Casapia, J. L. S., Merma Aruhuanca, L., Rejas, M. H. (2019). Evaluación de la concentración de polvo atmosférico sedimentable y material particulado (PM2.5, PM10) para la gestión de la calidad del aire 2017, en la ciudad de Tacna. *Ingeniería Investiga, 1*(1), 124–138. https://revistas.upt.edu.pe/ojs/index.php/ingenieria/article/view/128
26. Organización Mundial de la Salud (OMS). (2021). *WHO global air quality guidelines. In Particulate matter (PM2.5 and PM10), ozone, nitrogen dioxide, sulfur dioxide and carbon monoxide.* https://www.who.int/publications/i/item/9789240034228
27. Rodriguez, M. G., Heredia Rivera, B., Rodriguez Heredia, M., Rodriguez Heredia, B., Gonzalez Segovia, R. (2019). A study of dust airborne particles collected by vehicular traffic from the atmosphere of southern megalopolis Mexico City. *Environmental Systems Research, 8*(1), 16. https://doi.org/10.1186/S40068-019-0143-3
28. Santillán-Lima, P., Llerena, M. R., Santillán-Lima, J., Molina-Granja, F., Caichug-Rivera, D., Lozada-Yánez, R. (2023). Assessment of the concentration of settleable particulate matter using geographic information systems in the central Ecuadorian highlands. *EAI Endorsed Transactions on Scalable Information Systems, 11*(3), 1–10. https://doi.org/10.4108/EETSIS.4156
29. Servicio Nacional de Meteorología e Hidrología del Perú (SENAMHI). (2025). *Memoria Institucional Anual 2024*. https://www.senamhi.gob.pe/pdf/trans/memoria-senamhi-2024.pdf